Plasma Sci. Technol. **26** (2024) 075501 (7pp) https://doi.org/10.1088/2058-6272/ad2d10

Gliding arc discharge in combination with Cu/Cu_2O electrocatalysis for ammonia production

Xue LIU (刘学)[1,2], **Jiawei ZHANG** (张佳伟)[1,2], **Yi HE** (何弈)[1,2], **Jiamin HUANG** (黄嘉敏)[1,2], **Xiaoping MA** (马晓萍)[1,2], **Xiaoman ZHANG** (张潇漫)[1], **Manting LU** (卢曼婷)[1,2] **and Yu XIN** (辛煜)[1,2,*]

[1] Jiangsu Key Laboratory of Thin Films, School of Physical Science and Technology, Soochow University, Suzhou 215006, People's Republic of China
[2] Jiangsu Key Laboratory of Advanced Negative Carbon Technologies, Soochow University, Suzhou 215123, People's Republic of China

[*]E-mail of corresponding author: yuxin@suda.edu.cn

Received 4 January 2024, revised 20 February 2024
Accepted for publication 26 February 2024
Published 27 June 2024

Abstract

Highly efficient and green ammonia production is an important demand for modern agriculture. In this study, a two-step ammonia production method is developed using a gliding arc discharge in combination with Cu/Cu_2O electrocatalysis. In this method, NO_x is provided by the gliding arc discharge and then electrolyzed by Cu/Cu_2O after alkaline absorption. The electrical characteristics, the optical characteristics and the NO_x production are investigated in discharges at different input voltage and the gas flow. The dependence of ammonia production through Cu/Cu_2O electrocatalysis on pH value and reduction potential are determined by colorimetric method. In our study, two discharge modes are observed. At high input voltage and low gas flow, the discharge is operated with a stable plasma channel which is called the steady arc gliding discharge mode (A-G mode). As lowering input voltage and raising gas flow, the plasma channel is destroyed and high frequency breakdown occurs instead, which is known as the breakdown gliding discharge mode (B-G mode). The optimal NO_x production of 7.34 mmol h^{-1} is obtained in the transition stage of the two discharge modes. The ammonia yield reaches 0.402 mmol h^{-1} cm^{-2} at pH value of 12.7 and reduction potential of −1.0 V versus reversible hydrogen electrode (RHE).

Supplementary material for this article is available online

Keywords: gliding arc discharge, nitrogen fixation, Cu/Cu_2O catalyst, electrocatalytic reduction of nitrite

(Some figures may appear in colour only in the online journal)

1. Introduction

Nitrogen is an essential component of all living things, which provides nutrition by consuming nitrogen in the form of organic compounds. With the introduction of the Haber-Bosch (H-B) process for industrial nitrogen fixation at the turn of the 20th century, food production became more dependent on nitrogen fertilizers, and food crop yields significantly increased [1–4]. Direct application of nitrogen fertilizer in the form of nitrate will cause nutrient loss and potentially environmental damage, whereas ammonium fertilizer has a quick and long-lasting effect on crops [5]. However, the H-B process relies heavily on non-renewable fossil fuels with a huge demand for hydrogen, and most of

* Author to whom any correspondence should be addressed.

all, it brings serious environmental pollution. Therefore, it is an urgent need to seek a highly efficient and green form of nitrogen fixation to realize modern agriculture [6].

Non-thermal plasma (NTP), due to the nature of its nonequilibrium state, is able to overcome the high energy barrier during N_2 excitation and activation, and its energy consumption for nitrogen fixation is lower than that of the standard ammonia synthesis as determined by thermodynamics [7, 8]. Based on this viewpoint, the interaction of nitrogen with oxygen or hydrogen to produce nitrogen oxide or ammonia is commonly used in plasma-based nitrogen fixation [9]. In addition to readily available nitrogen, ammonia production requires expensive hydrogen, and even if cheap water is used instead of hydrogen, but ammonia selectivity is limited [10, 11]. In contrast, the raw material (air) required for plasma generation of nitric oxide is both abundant and inexpensive. Thus, the promising way for ammonia production is the air plasma combined with electrocatalytic technology which resolves the difficulty of N_2 dissociation and achieves efficient ammonia conversion [12–15]. It fulfills the convenience of direct irrigation of ammonium fertilizer in agriculture.

Gliding arc discharge (GAD), including the characteristics of both thermal and non-thermal plasma, is usually viewed as one candidate of the most effective and promising plasmas for gas conversion [16]. Indeed, the average electron energy in the gliding arc is in the range of 0.6–4.0 eV, which is more beneficial for N_2 vibrational excitation than other plasmas [17]. Vibrationally excited nitrogen plays an important role in overcoming the high reaction energy barrier of the Zeldovich reactions (1)–(3) to form NO_x efficiently [18, 19].

$$e^- + N_2 \rightarrow e^- + N_2(v) \tag{1}$$

$$O + N_2(v) \rightarrow NO + N \tag{2}$$

$$NO + O \rightarrow NO_2 \tag{3}$$

Due to the subsequent combination with an electrocatalytic process, a higher NO_x yield in the gliding arc process should be more desirable. NO_x is absorbed by alkaline solution to generate NO_2^- which has a low electrolytic dissociation energy and requires fewer electrons for the conversion to ammonia compared to NO_3^- [20, 21]. Wang *et al* [17] investigated NO_x formation mechanisms with the ratio of N_2 and O_2 in a pulsed-power milliscale GAD reactor. The highest concentration of NO_x was achieved at a N_2/O_2 ratio of 80:20, which is very close to air composition. Moreover, NO_x decomposition after GAD process was restrained since the gas temperature drops quickly [22]. This once again shows that GAD with cheap and readily available atmospheric air can be an efficient and economical method for producing NO_x.

To improve NO_x production, the operating parameters (i.e., mainly gas flow and input voltage) of GAD have been extensively studied experimentally [23–26]. Chen *et al* [27] found that higher gas flow rate reduces the NO_x concentration, whereas increasing the input voltage slightly raises the NO_x concentration but increases energy consumption. Furthermore, the operating parameters not only affect the NO_x production, but also change the behavioral characteristics of the GAD. Relevant studies have investigated the discharge characterization of GAD at different operating parameters. Lei *et al* presented the arc motion images taken by a high-speed camera and confirmed the existence of two different gliding discharge modes: the breakdown gliding discharge mode (B-G mode) and the steady arc gliding discharge mode (A-G mode) [28, 29].

To our knowledge, the discharge channel of gliding arc is accompanied by the generation of active particles, the production of NO_x is actually directly related to the discharge modes. Thereby, we have attempted to gain better insights into the relationship between the discharge mode of GAD and NO_x production, which enables us to quickly find out the optimal parameters for the intermediate NO_x for ammonia synthesis in gliding arc discharge.

The catalyst materials required in electrocatalytic nitrate reduction for ammonia generation have also gained increasing attention [30–33]. Among the various catalysts, copper has the dual advantages of low cost and high activity. The presence of its large number of unpaired d-orbital electrons, moderate intermediate adsorption barriers, and inhibition of the hydrogen-extraction reaction (HER) on copper-based materials has been widely investigated [34]. In particular, the oxide-derived Cu-based catalysts prepared by electrochemical reconstruction exhibited enhanced NH_3 selectivity during NO_3^- reduction. Compared with pure copper, the electron transfer at the Cu/Cu_2O interface favors the formation of *NOH key reaction intermediates during nitrite reduction and inhibits the competitive generation of H_2 [35–37].

In this study, a two-step process for ammonia production is proposed using GAD and electrocatalytic technology. In the experimental setup, the electrical characteristics and arc dynamics of the discharge were investigated under different operating conditions. For better understanding the correlation between discharge behavior and NO_x production, the optical characteristics and the electrical characteristics are carried out. On the other hand, the reaction conditions in the process of Cu/Cu_2O electrocatalytic reduction of nitrite were optimized, so as to ensure the efficient formation of ammonia in the final product.

2. Experimental section

Schematic apparatus, including discharge system to generate NO_x and a system of electrocatalytic reduction, is shown in figure 1. The gliding arc discharge system uses a high-voltage sinusoidal power supply (CTP-2000K) with a frequency of 9 kHz, and the outputs of the power supply are connected to the gliding arc reactor. The gliding arc reactor consists of two identical graphite electrodes with a 40 mm

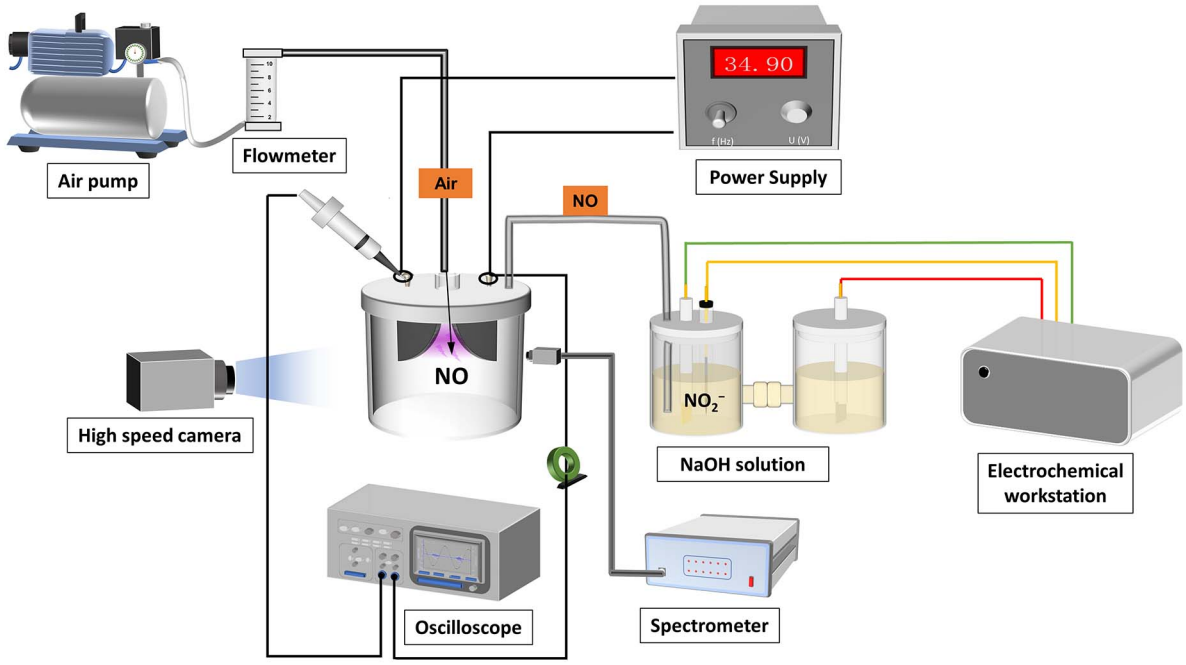

Figure 1. Schematic diagram of experimental process.

radius placed opposite each other. The smallest distance between the two blade electrodes is set to be 2.0 mm. The two electrodes are connected to high-voltage and ground terminal, respectively. The compressed air is introduced by using a mass flow meter. A high-speed camera ICCD is used to capture the evolution of the gliding arc discharge. During the discharge, the discharge voltage and current waveform of the discharge are measured using a high voltage probe (P6015A, Tektronix) and a current probe (TCP0030, Tektronix) connected to the oscilloscope, respectively. The reaction products are introduced from the reactor into a gas-wash bottle and partially converted to ions such as NO_2^- in solution using liquid absorption.

The electrocatalytic reduction reaction is performed on a custom-designed 50 mL H-type electrochemical tank. Constant potential is carried out using a CS2350H (Wuhan Corrtest Instruments Corp., Ltd.) electrochemical workstation, with the cathode and anode chambers separated by a Nafion@117 membrane. The working electrode (WE) is a prepared Cu/Cu_2O nanowire arrays (NAs) (figure S4) with a working area of 1.0 cm^2, an Ag/AgCl (Sat) electrode is used as the reference electrode (RE), and a platinum sheet as the counter electrode (CE).

3. Result and discussion

Two discharge modes exist during the gliding arc discharge process, a breakdown gliding discharge mode called B-G mode and a steady arc gliding discharge mode called A-G mode, which strongly depend on discharge power and input airflow.

Figure 2 shows a typical discharge *V&I* waveform including A-G mode and B-G mode during gliding arc discharge process [38], and their photos taken by CCD camera are shown in the inset of figure 2(a). The left part in figure 2(a) mainly represents the A-G mode, and the discharge voltage waveform displays a periodic sinusoidal signal with the current in a few milliamperes. During the A-G mode, the arc basically stabilizes near a certain position as observed with ICCD shown in figure 2(b). The right part of the figure 2(a), which mainly represents the B-G mode, reveals that the discharge voltage waveform deviates seriously from the one in the A-G mode, the discharge current shows many pulsed spikes with amplitude of the order of amperes. During the B-G mode as shown in figure 2(c), the initial arc is onset at the narrowest distance of the electrode and then moves significantly downward, eventually extinguishes, and subsequently the next arc proceeds.

Figure 3 clearly illustrates the effect of input voltage (U_0) on the mode transition of the discharge with air gas flow rate of 1.0 L min^{-1}, in which the blue and purple blocks represent the proportions of A-G and B-G modes during the whole discharge, respectively. We can roughly estimate the proportion of discharge modes based on the magnitude of discharge current for discharge duration of 2 s as shown in figure 3(d). It is clearly seen that increasing input voltage causes the mode transition of the gliding arc discharge with B-G mode proportion from 99.64%@60 V to 13.71%@120 V, while A-G mode from 0.36%@60 V to 86.29%@120 V, a similar scissor difference structure.

Air flow rate can also exert impact on the discharge mode transition as shown in figure 4. When the gas flow rate keeps low, the gliding arc discharge mode is basically in the

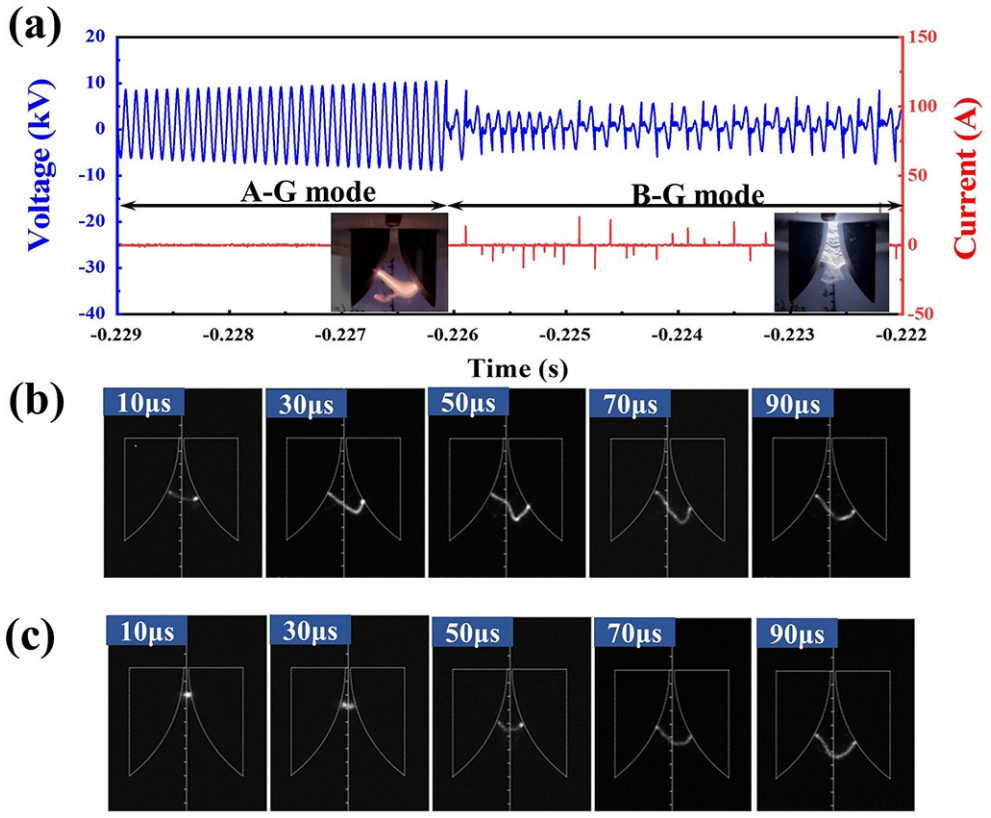

Figure 2. (a) Discharge voltage and current waveforms of gliding arc discharge. The time interval ICCD images of (b) A-G mode and (c) B-G mode for flow rate of 1.5 L min^{-1} and input voltage of 100 V.

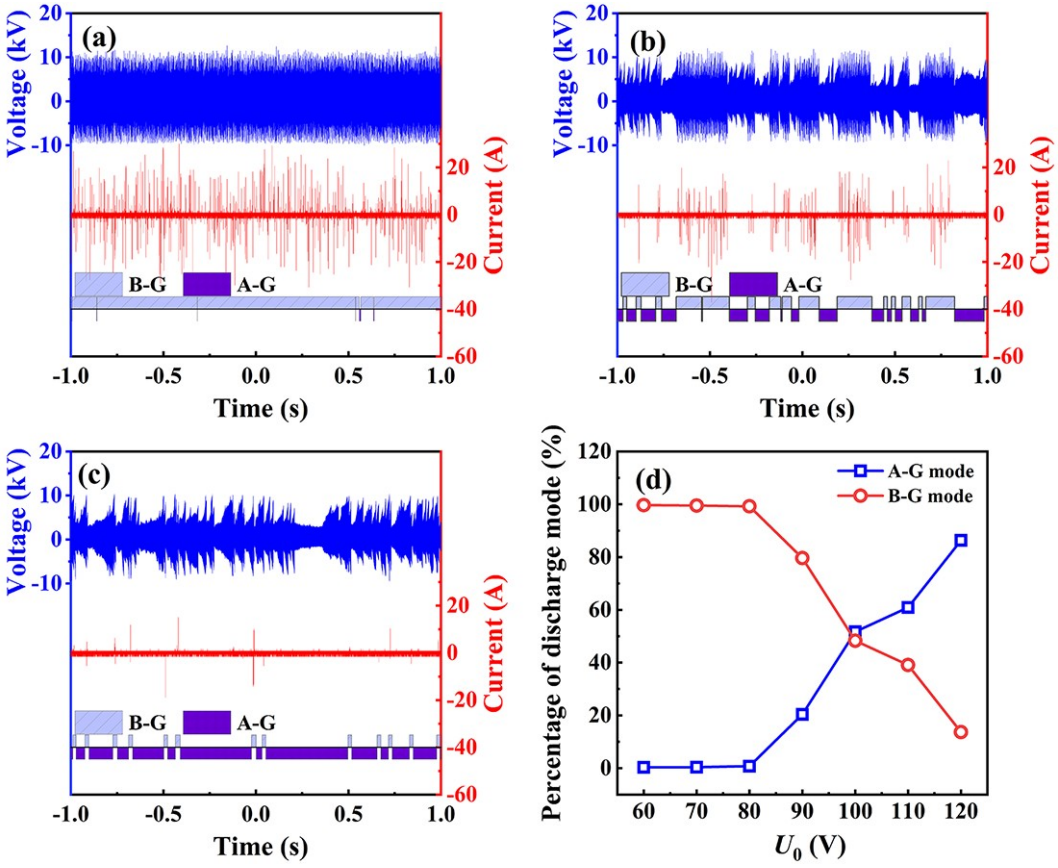

Figure 3. Discharge voltage and current waveforms of gliding arc discharge with flow rate of 1.0 L min^{-1} at different input voltages U_0 of (a) 80 V, (b) 100 V, (c) 120 V; (d) the percentage of the discharge mode.

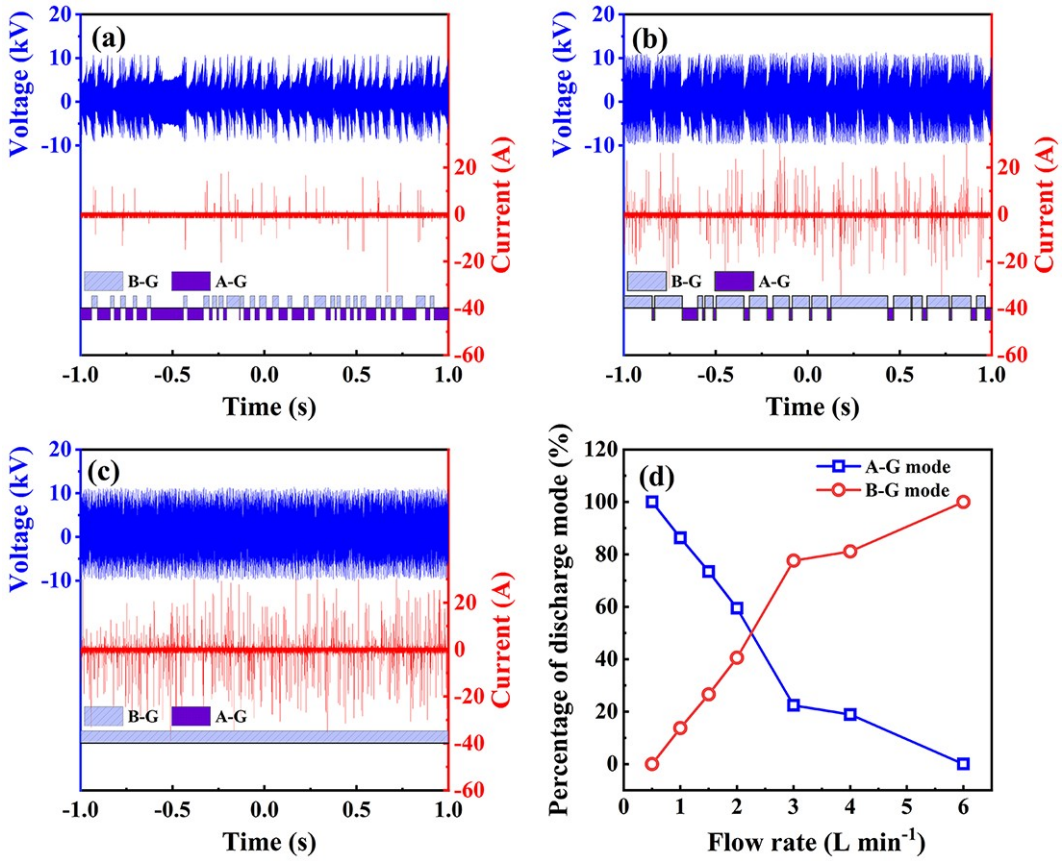

Figure 4. Discharge voltage and current waveforms of gliding arc discharge with input voltage of 120 V at different airflow rates of (a) 2.0 L min^{-1}, (b) 4.0 L min^{-1}, (c) 6.0 L min^{-1}; (d) the percentage of the discharge mode.

state of A-G mode. With the gas flow rate increasing to 6.0 L min^{-1}, the gliding arc discharge mode gradually shifts to the B-G mode as shown in figures 4(b) and (c), in which both the breakdown frequency and the amplitude of the pulsed current rise. Figure 4(d) shows the evolution of the proportion for the two modes with air flow rate, also another similar scissor difference structure.

In the transition process of A-G and B-G mode, the energy input and dissipation of the gliding arc play a crucial role [39]. The magnitude of the input voltage directly determines the amount of input energy between the electrodes, while the control of air flow rate affects the transfer speed of heat and mass in the gliding arc [40–42]. When the input voltage increases, the input energy between the electrodes also increases, promoting the arc to develop into a stable A-G mode discharge state. On the contrary, when the air flow rate increases, the airflow will accelerate the heat and mass transfer process of the arc, causing the arc to slide downwards and gradually elongate. During this process, a large number of electrons/ions and neutral particles in the channel diffuse and drift, promoting the arc to transition to B-G mode discharge [39]. At the same time, the breakdown frequency and current will also increase accordingly. As the arc slides downwards, the distance between the electrodes gradually increases, resulting in a decrease in the density of electron ions between the electrodes. This increases the relative resistance, ultimately leading to insufficient input power energy to sustain the continuous combustion of the arc channel [43]. At the end of the arc cycle, a new arc will be excited again at the narrowest point of the electrode, generating conductive particles and repeating this process [28, 29].

Different discharge modes of the gliding arc obviously affect the concentration of active particles and even nitrogen fixation efficiency. Among these, vibrational excited nitrogen ($N_2(v)$) plays an important role in overcoming the high reaction energy barrier of the Zeldovich reactions (1)–(3) to form NO_x efficiently [18, 19]. Here, the band head of N_2 second-positive systems (SPS) $N_2(C^3\Pi_u \rightarrow B^3\Pi_g)$ in the optical emission spectroscopy can be used as an indicator of active precursor qualitatively to disclose the dependence of input power and air gas flow rate on the $N_2(v)$ during gliding arc discharge [29]. Additionally, the formed nitrogen oxide during arc discharge is converted to the NO_2^- radical by absorption from alkaline solutions with pH value of 12.7 to facilitate subsequently electrocatalytic reduction to ammonia. The detection of NO_2^- yield using the colorimetric method is also equivalent to the amount of NO_x produced by the gliding arc (figure S5).

Figure 5 shows the dependence of $N_2(v)$ emission intensity (hollow circle) and NO_2^- concentration generated through alkaline absorption (hollow triangle) on input voltage under different air flow rates. The column chart shows the proportion of the two modes under different discharge conditions, in which the light grey and the dark grey

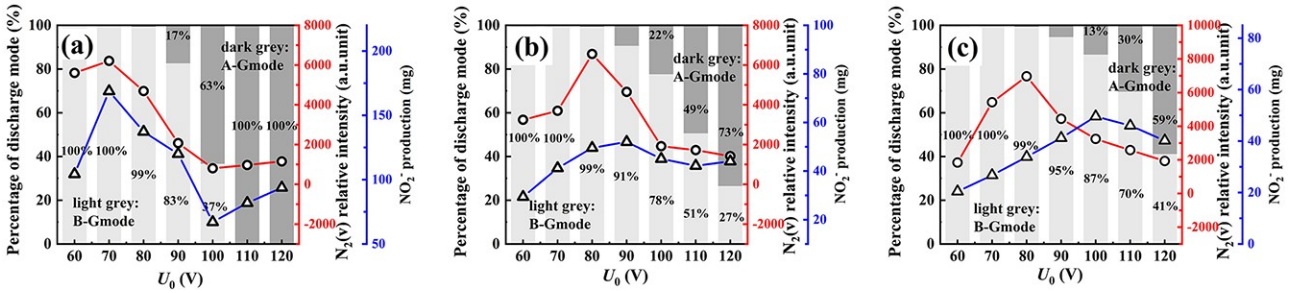

Figure 5. The percentage of the discharge mode, $N_2(C^3\Pi_u \rightarrow B^3\Pi_g)$ relative emission intensities and the production of NO_2^- at different input voltages under (a) 0.5 L min^{-1} (b) 1.5 L min^{-1} and (c) 2.0 L min^{-1} for 30 min.

columns represent B-G mode and A-G mode proportions, respectively. It seems that positive correlation exists with a certain voltage between intensity of $N_2(v)$ and NO_2^- concentration in the solution. Additionally, it can also be found that the occurrence of peak concentration falls between A-G and B-G modes. But the increase in gas flow rate leads to a poor correlation of the $N_2(v)$ intensity and NO_2^- concentration shown in figure 5(c). Figure 6 also shows that under high input voltage, this poor correlation exhibits a greater deviation with increasing flow rate. A higher flow rate resulted in a lower NO_x yield, which is in agreement with the result of Vervloessem *et al* [22]. The reason for this deviation may be caused by rapid quenching of $N_2(v)$ or short reaction time with active oxygen [44, 45]. Kossyi *et al* [45] found that the lifetime of N_2 excited state can reach the microsecond scale in the absence of O_2, while presence of O_2 causes lifetime of N_2 on the nanosecond scale due to recombination and ionization.

In the B-G mode, the arc is unstable with high-frequency breakdown compared with the stable arc in the A-G mode. High gas flow and low input voltage restrain the absorbed energy to form a stable arc and make the discharge turn to the B-G mode. To our knowledge, the breakdown process may be helpful to the production of $N_2(v)$. Actually, in our experiment, the maximum NO_2^- production with 7.34 mmol h^{-1} converted by NO_x in GAD occurs at gas flow rate of 0.5 L min^{-1} and input voltage of 70 V.

Ammonia fertilizer is a more efficient fertilizer during crop growth compared to other nitrogenous fertilizers such as nitrite. Therefore, by using self-made Cu/Cu_2O catalyst, we have attempted to use an H-type cell to realize a conversion of NO_2^- formed by dissolution of NO_x generated by gliding arc discharge in alkaline solution. Compared to pure copper, the electron transfer at the Cu/Cu_2O interface is beneficial for the formation of key intermediate products *NOH during nitrite reduction and inhibits the competitive reaction of H_2. Theoretical calculations and some experiences have shown that different crystalline surfaces of copper can be affected by pH value, with Cu (100) crystalline surfaces having higher catalytic activity for nitrate reduction to ammonia in strongly acidic environments, while in neutral or alkaline environments Cu (111) has a higher catalytic activity [46–50]. In our experiment, the fabrication of Cu/Cu_2O catalyst is followed by the work of Sun's group [15] as shown in figure S4.

In our experiments, the pH value, reduction potentials, and reactant concentrations are adjusted to achieve the optimum ammonia yield. We have noticed that the concentration of NaOH solution with the pH value more than 12.0 will capture more NO_x efficiently formed in the gliding arc discharge (figure S9). Our results show that ammonium yield can be generated up to 0.402 mmol h^{-1} cm^{-2} with high Faradaic efficiency at pH of 12.7 and potential of −1.0 V versus RHE. The use of alkaline solution as the electrolyte not only absorbs the intermediate product NO_x in the gliding arc process, but also reduces the side reaction in the reduction of NO_2^- to ammonia, such as the byproduct of N_2 and H_2.

To view from figure 7(a), it is found that the ammonia

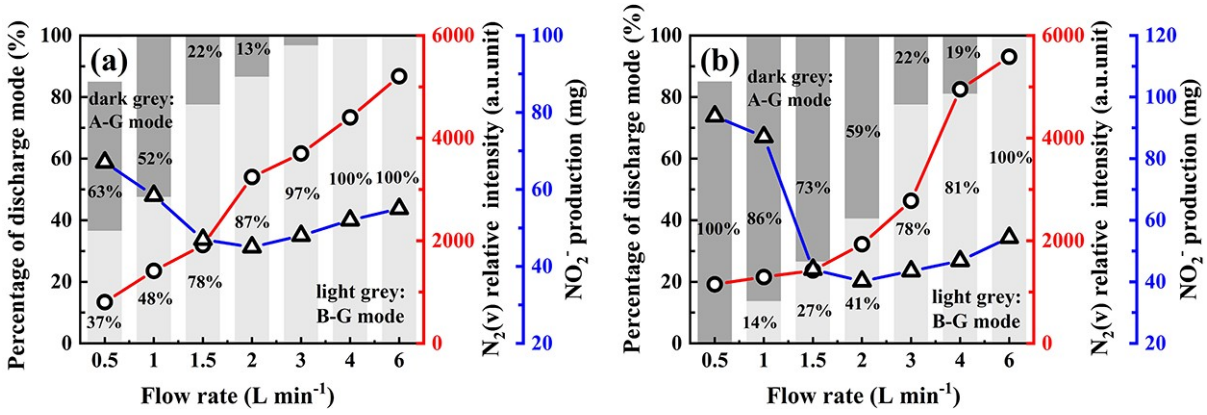

Figure 6. The percentage of the discharge mode, $N_2(C^3\Pi_u \rightarrow B^3\Pi_g)$ relative emission intensities and the production of NO_2^- at different flow rates in (a) 100 V, (b) 120 V for 30 min.

production rate of electrocatalysis utilizing 1.0 cm^2 of Cu/Cu_2O is much lagged behind than the NO_2^- yield of gliding arc in our experiment. A large amount of NO_2^- will accumulate in the electrolyte and cannot be converted promptly. Therefore, it is necessary to match the catalyst area of appropriate size with the generated NO_2^- concentration. It can be found that, with electrode area increasing, the production rate of NH_4^+ increases while that of NO_2^- decreases, and the accumulation of NO_2^- nearly disappears with the Cu/Cu_2O catalyst area of 16.0 cm^2, suggesting efficient conversion of NH_4^+. The electrocatalytic conversion of NO_x in discharge to NH_4^+ reaches 87.19%.

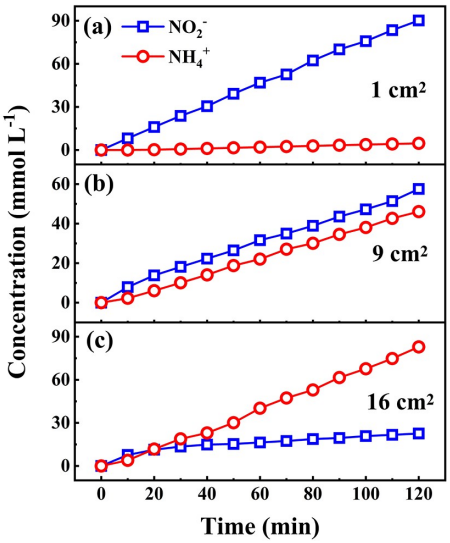

Figure 7. NO_2^- and NH_4^+ concentration with time for the gliding arc discharge in different Cu/Cu_2O areas of (a) 1.0 cm^2, (b) 9.0 cm^2 and (c) 16.0 cm^2.

4. Conclusions

Ammonia production method is developed using a gliding arc discharge in combination with Cu/Cu_2O electrocatalysis. Firstly, the electrical characteristics, the optical characteristics and the NO_x production of A-G mode and B-G mode are investigated. The two discharge modes are operated via the manipulation of the input voltage and the gas flow. In the B-G mode, low input voltage and high gas flow makes the arc unstable with high-frequency breakdown, while in the A-G mode, the arc keeps stable with high input voltage and low gas flow. In the B-G mode, the high-frequency breakdown promotes the production of $N_2(v)$. In considering $N_2(v)$ quenching and short reaction time with active O, the optimal $N_2(v)$ production and NO_x yield of gliding arc are in the transition stage between B-G mode and A-G mode with input voltage of 70 V and gas flow rate of 0.5 L min^{-1} in our experiment. The alkaline electrolyte effectively absorbs the NO_x produced by the gliding arc to convert to nitrite in it and electrocatalytic experiments show a high yield 0.402 mmol h^{-1} cm^{-2} at a potential of −1.0 V versus RHE. Finally, it is revealed that the efficient conversion of NH_4^+ is obtained as long as the accumulation of NO_2^- is suppressed by enlarging the electrode area. Our experiment may provide some new ideas for continuous ammonium fertilizer application in modern agriculture.

References

[1] Dawson C J and Hilton J 2011 *Food Pol.* **36** S14
[2] Ranieri P *et al* 2021 *Plasma Processes Polym.* **18** 2000162
[3] Erisman J W *et al* 2008 *Nat. Geosci.* **1** 636
[4] Pfromm P H 2017 *J. Renewable Sustain. Energy* **9** 034702
[5] Lassaletta L *et al* 2014 *Environ. Res. Lett.* **9** 105011
[6] MacFarlane D R *et al* 2020 *Joule* **4** 1186
[7] Cherkasov N, Ibhadon A O and Fitzpatrick P 2015 *Chem. Eng. Process.: Process Intensif.* **90** 24
[8] Chen H *et al* 2021 *Waste Dispos. Sustain. Energy* **3** 201
[9] Chen J G *et al* 2018 *Science* **360** eaar6611
[10] Burlica R, Kirkpatrick M J and Locke B R 2006 *J. Electrostat.* **64** 35
[11] Gorbanev Y *et al* 2020 *ACS Sustain. Chem. Eng.* **8** 2996
[12] Li W Y *et al* 2023 *ACS Sustain. Chem. Eng.* **11** 1168
[13] Wu A J *et al* 2021 *Appl. Catal. B: Environ.* **299** 120667
[14] Li L Q *et al* 2021 *Angew. Chem. Int. Ed.* **60** 14131
[15] Sun J *et al* 2021 *Energy Environ. Sci.* **14** 865
[16] Rouwenhorst K H R *et al* 2020 *Green Chem.* **22** 6258
[17] Wang Z F *et al* 2022 *Plasma Sources Sci. Technol.* **31** 05LT01
[18] Fridman A *et al* 1999 *Prog. Energy Combust. Sci.* **25** 211
[19] Rouwenhorst K H R *et al* 2021 *Energy Environ. Sci.* **14** 2520
[20] Tsonev I *et al* 2023 *ACS Sustain. Chem. Eng.* **11** 1888
[21] Patil B S *et al* 2016 *Appl. Catal. B: Environ.* **194** 123
[22] Vervloessem E *et al* 2020 *ACS Sustain. Chem. Eng.* **8** 9711
[23] Zhang C *et al* 2017 *IEEE Trans. Dielectr. Electr. Insul.* **24** 2148
[24] Chen Z *et al* 2021 *J. Phys. D: Appl. Phys.* **54** 225203
[25] Ananthanarasimhan J *et al* 2021 *IEEE Trans. Plasma Sci.* **49** 502
[26] Zhang H *et al* 2016 *Plasma Sci. Technol.* **18** 473
[27] Chen H *et al* 2021 *Plasma Processes Polym.* **18** 2000200
[28] Lei J P *et al* 2020 *Acta Phys. Sin.* **69** 195203 (in Chinese)
[29] Hu C H *et al* 2021 *J. Phys. D: Appl. Phys.* **54** 205202
[30] Yang W J *et al* 2022 *Sep. Purif. Technol.* **295** 121278
[31] Gao J N *et al* 2019 *Appl. Catal. B: Environ.* **254** 391
[32] Zhang Y Z *et al* 2022 *Appl. Catal. B: Environ.* **310** 121346
[33] Xu H *et al* 2022 *Chem. Soc. Rev.* **51** 2710
[34] Zhou N *et al* 2023 *ACS Catal.* **13** 7529
[35] Shen Z R *et al* 2023 *ACS Sustain. Chem. Eng.* **11** 9433
[36] Chen Q Y *et al* 2022 *Chem. Commun.* **58** 517
[37] Wang Y T *et al* 2020 *Angew. Chem. Int. Ed.* **59** 5350
[38] He L M *et al* 2016 *High Voltage Eng.* **42** 1921 (in Chinese)
[39] Cheng X Y *et al* 2022 *Plasma Sci. Technol.* **24** 115502
[40] Wang W Z *et al* 2016 *Plasma Sources Sci. Technol.* **25** 065012
[41] Kalra C S, Gutsol A F and Fridman A A 2005 *IEEE Trans. Plasma Sci.* **33** 32
[42] El-Zein A *et al* 2016 *IEEE Trans. Plasma Sci.* **44** 1155
[43] Sun S R *et al* 2017 *Plasma Sources Sci. Technol.* **26** 055017
[44] Liu J L *et al* 2023 *Plasma Processes Polym.* **20** e2300153
[45] Kossyi I A *et al* 1992 *Plasma Sources Sci. Technol.* **1** 207
[46] Hu T *et al* 2021 *ACS Catal.* **11** 14417
[47] Zhao Y L *et al* 2022 *Nano Energy* **97** 107124
[48] Fang J Y *et al* 2023 *Materials* **16** 4000
[49] Pérez-Gallent E *et al* 2017 *Electrochim. Acta* **227** 77
[50] Barrera L *et al* 2023 *ACS Catal.* **13** 4178